10-15-2018

The effect of ionic liquid adsorption on the electronic and optical properties of fluorographene nanosheets

Mehdi Shakourian-Fard
Birjand University of Technology

S. Maryamdokht Taimoory
University of Windsor

Volodymyr Semeniuchenko
University of Windsor

Ganesh Kamath
Dalzierfiver LLC

John F. Trant
University of Windsor

The Effect of Ionic Liquid Adsorption on the Electronic and Optical Properties of Fluorographene Nanosheets

Mehdi Shakourian-Fard[a*], S. Maryamdokht Taimoory[b*], Volodymyr Semeniuchenko[b], Ganesh Kamath[c], John F. Trant[b*]

[a]Birjand University of Technology, Department of Chemical Engineering, Birjand, P.O. Box 97175/569, Iran.
[b]University of Windsor, Department of Chemistry and Biochemistry, Windsor, Canada.
[c]Dalzierfiver Inc 3500 Carlfied St EL Sobrante CA 94803.

Corresponding authors: E-mail: shakourian@birjandut.ac.ir

E-mail: j.trant@uwindsor.ca

E-mail: taimoory@uwindsor.ca

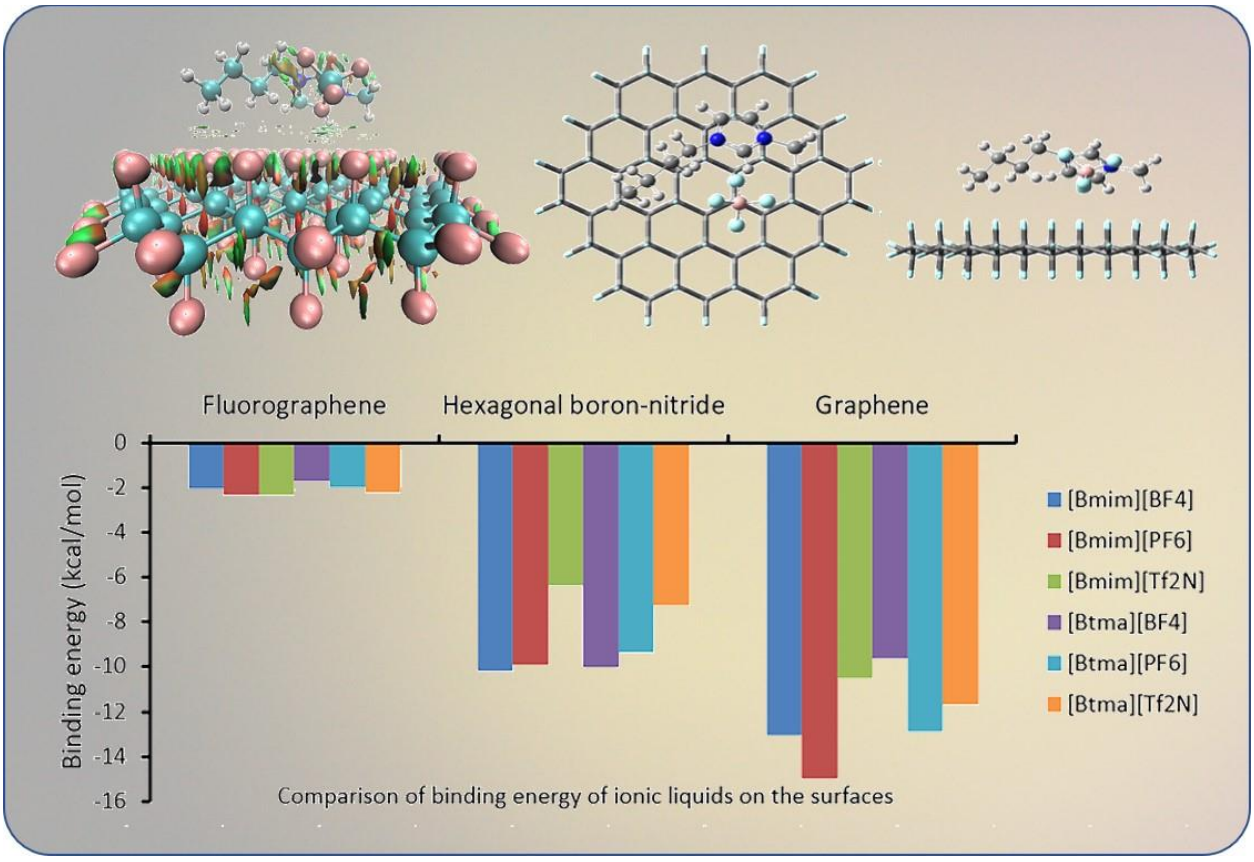

Abstract

In the present study, we investigate the adsorption characteristics of six different ionic liquids (ILs) on a fully-fluorinated graphene (fluorographene, FG) surface using electronic structure studies and associated analysis methods. A systematic comparison of differences in IL binding energies (ΔE_b) with fluorographene, graphene and hexagonal boron nitride surfaces indicates that fluorination strongly decreases the binding energy compared to the other two surfaces, hence resulting in the binding energetics: $\Delta E_{b\ (Graphene\ldots IL)} > \Delta E_{b\ (Hexagonal\ boron\text{-}nitride\ldots IL)} > \Delta E_{b\ (Fluorographene\ldots IL)}$. To probe the reasons for this difference, quantum theory of atoms in molecules (QTAIM) analysis and non-covalent interactions (NCI) analyses were carried out. Results indicate that the stability of complexes of FG surface with ILs (FG…IL) arises only due to the presence of the expected weak non-covalent intermolecular interactions. The calculation of charge transfers by employing the ChelpG method shows that the interaction of ILs with FG surface generally induces a negative charge on the FG surface. Furthermore, these interactions lead to a decrease of the HOMO-LUMO energy gap (E_g) of the FG surface, enhancing its electrical conductivity. In addition, a detailed analysis of the global molecular descriptors including the Fermi energy level (E_{FL}), work function (WF), electronic chemical potential (μ), chemical hardness (η), global softness (S) and electrophilicity index (ω) was carried out for both the FG surface alone and the adsorbed complexes showing that there are small, but meaningful, differences in the reactivity of the surface depending on the nature of the IL. Finally, time-dependent DFT (TD-DFT) calculations of the optical properties of FG surface and FG…IL complexes reveal that the absorption spectrum of the FG surface undergoes a red shift following IL adsorption. This study demonstrates that FG provides a useful complementary tool to graphene and boron nitride materials, allowing for the fine-tuning of the optoelectronic properties of these monolayer materials. These results will assist in the development of these types of ILs for applications in optoelectronics.

Keywords: Ionic liquid, Fluorographene nanosheet, Optical properties, Adsorption, DFT calculations, Non-covalent interactions

1. Introduction

Graphene, a two-dimensional (2D) material, has generated considerable interest for its potential for (opto)electronic applications, including as the basis for gas sensing systems [1], electrochemical energy storage [2] DNA sequencing [3] coating technologies [4] and functional composites [5]. Although graphene's zero band gap hinders its performance in microelectronic device applications, a suitable band gap can be created through chemical functionalization; this allows for the required fine-tuning of the electronic and magnetic properties of 2-D nanomaterials for future applications in microelectronics [6]. Recently, covalently modified graphene derivatives prepared by derivatization with hydrogen, the halogens, and other atoms have attracted considerable interest for their potential applications in electronic devices [7-9]. Fluorographene (FG) is a fluorocarbon derivative of graphene: all carbon atoms are sp^3 hybridized through the

incorporation of polar C-F bonds. The change of hybridization from sp^2 in graphene, to sp^3 in fluorographene, preserves the two-dimensional hexagonal symmetry, but significantly changes the physical, chemical, electrical and electrochemical properties and local structure of the material. This induces an opening of the band gap to a non-zero value as it involves a loss of the fully-delocalized π electron system [10].

Fluorographene can be used as a tunnel barrier and as a high-quality insulator or barrier material for organic electronics. It can also act as a wide-gap semiconductor in light-emitting diodes (LEDs) and displays [11]. Fluorographene can be synthesized from graphene (e.g., exfoliated graphene, reduced graphene oxide (RGO), graphene grown by chemical vapor deposition (CVD) on silicon-on-insulator substrate) by treatment with fluorinating agents, including xenon difluoride (XeF_2), fluorine (F_2) gas, or fluoropolymers. The sp^2-hybridized carbon atoms of the graphene lattice react with these F• equivalents, forming C-F sp^3 bonds and producing fluorinated graphenes [12]. Fluorographene can also be readily prepared from graphene oxide *via* photochemical fluorination [13] or plasma treatment [14]. Graphene oxide has been fluorinated through solvothermal or hydrothermal fluorination using precursors such as BF_3-etherate [15], hydrofluoric acid (HF) [16], hexafluorophosphoric acid (HPF_6) [17], and diethylaminosulfur trifluoride (DAST) [18].

The atomic ratio of carbon to fluorine ($R_{(C/F)}$) in the synthesis of fluorinated graphene affects the bandgap of fluorographene semiconductors which may play a vital role in emerging graphene-based molecular electronics and optoelectronics. The $R_{(C/F)}$ ratio in the synthesis of fluorinated graphene can be controlled by tuning the reaction conditions. For example, Wang et al. [16] presented an easy, low-cost and effective method for the synthesis of fluorinated graphene with tunable $R_{C/F}$ by the reaction between dispersed graphene oxide and hydrofluoric acid. Their results showed that fluorine is grafted onto the basal plane of graphene, and the $R_{C/F}$ can be easily adjusted by modifying the reaction conditions such as fluorination temperature, reaction time, reaction pH and the number of equivalents of fluorinating agents. By controlling the fluorination reaction conditions, they obtained the $R_{(C/F)}$ = 2.1 for their synthesized fluorinated graphene surface. However, fully fluorinated graphene surface has also been synthesized by several research groups [11, 19-22], and is both thermally stable at up to 400 $^{\circ}$C in air [11] and chemically inert.

Liquid-phase exfoliation of 2D materials is one of the most promising routes for their production on a large scale [23]. Recently ionic liquids (ILs) have been used to mediate exfoliation as they

also improve the electronic behaviour of the resulting nanosheets and so can be used as both an exfoliant during manufacture, and as a coating for the eventual application [10,24]. The unique physicochemical properties of ILs such as their low melting point (below 100 °C), wide electrochemical window, high ionic conductivity, nonflammability, low vapor pressure, hydrophobicity, high ion density, and good thermal stability have been leading to an increasing number of their applications in Li-ion batteries, supercapacitors, solar cells, and proton exchange membranes in fuel cells [25-27].

The interactions at the interfacial layers between ionic liquids and nanomaterials is of paramount importance for the synthesis (exfoliation) of these 2D sheets [10,24], and for determining their optoelectronic appropriateness for emerging energy applications including as supercapacitors [28], ionic-liquid gated transistors [29], light-emitting diodes (LEDs) and displays [11]. The most studied system involves the surface interactions between ionic liquids and graphene. The resulting complexes have been studied both using experimental [30-31] and computational approaches [28-31]. The effect on 32-35]. On the other hand, the surface morphology is obviously different in the presence of a single molecule of the IL compared to a cluster such as a nanodroplet. Graphene-based monolayers tend to fold in the presence of ionic liquid nanodroplets and this effect has been quantified through contact angle measurements by Atilhan and co-workers [32-33].et al [36-37]. They have also reported studies explaining this ionic liquid-induced folding for graphene nanoribbons (GNRs), rectangular flakes and flower-like flakes using classical molecular dynamics simulations. The extent of the folding and the precise morphologies obtained are dependent on both the structure of the ionic liquid, the size of the nanodroplet, and the exact morphology of the graphene-based material. However, a more detailed analysis of nanodroplet-based interactions with fluorographene is beyond the scope of this current report, although studies are currently underway by our groups to look at the effect of IL nanodroplet interactions with the fluorographene surface. However, before progressing to these more complex systems, we require a fundamental understanding of the basic details of the fluorographene-IL interactionstrong interactions in flake-SiO_2 structure, hence synthesizing novel ILs was required.

Therefore, to fully realize the potential of ionic liquids as exfoliation solvents and electrolytes with FG, there is a pressing need to understand their interaction with FG at the electronic structure

and atomic scale. To date, however, very little is known about the nature of ionic liquid adsorption on fluorographene sheets.

We wish to report on our investigations into this potentially useful interaction. In the present report, we determine the specifics of the interaction of ionic liquids with fluorographene and compare the affinities of different ionic liquids (both 1-butyl-3-methylimidazolium $[Bmim]^+$, and butyltrimethylammonium $[Btma]^+$-based ILs) for the fluorographene surface using density functional theory (M06-2X/cc-pVDZ) method (Figure 1). ILs based on $[Bmim]^+$ and $[Btma]^+$ cations were selected because they have been used in the synthesis of fluorographene and other nanomaterials through exfoliation [10,24]. In addition, these classes of ILs have also been extensively used either as either the electrolyte, or as part of a composite electrode material, in nanomaterial-based supercapacitors, semiconductors, transistors, lithium ion batteries, fuel cells, and solar cells [24-29]. Finally, the emergent properties obtained in this study are compared with those we have previously calculated for graphene and boron nitride surfaces to show the complementarity of these three systems for developing innovative materials for 2-D semiconductor applications.

2. Computational details

$C_{54}F_{72}$ was chosen as a suitable initial model for fluorographene (FG). This FG model contains 54 carbon and 72 fluorine atoms. The edge carbon atoms are passivated with fluorine atoms. This model has been recently used by others to study the interaction between fluorographene surface and organic molecules [38]. All calculations are performed using the M06-2X density functional, which has been widely used to study the structure and energetics of similar weakly bonded systems [39-45]. In addition, the M06-2X functional has previously been used for investigation of interaction of ILs with hexagonal boron nitride [39], graphene [40] and boron nitride nanotube [44] surfaces in literature. This functional is more reliable than the B3LYP hybrid functional for predicting weak van der Waals interactions because the M06-2X functional uses 54% HF exchange energy, which is not well described by the non long-range corrected DFT methods. In this study, the M06-2X functional is applied to the system using Dunning's correlation consistent-polarized valence double zeta basis set (cc-pVDZ). All geometries of the FG model, ionic liquids (ILs; [Bmim][Y] and [Btma][Y] (Y = BF_4^-, PF_6^-, and Tf_2N^-) and the resulting FG…IL complexes were optimized with this M06-2X/cc-pVDZ level of theory. Calculated vibrational frequencies were

determined without imaginary frequencies to ensure the obtained structures are indicative of FG…IL complex energy minima. The binding energies (ΔE_b) were calculated using Equation 1:

$$\Delta E_b = E_{FG...IL} - (E_{FG} + E_{IL}) + E_{BSSE} \qquad \text{(Equation 1)}$$

where E_{FG}, E_{IL} and $E_{FG...IL}$ denote the total energies of the FG model, ILs and $E_{FG...IL}$ complexes, respectively. For optimized structures, the last term ($E_{FG...IL}$) was corrected according to basis set superposition error (BSSE) through the counterpoise procedure [46] as follows:

$$E_{FG...IL} = E_{FG...IL,\ uncorrected} + E_{CC} \qquad \text{(Equation 2)}$$

The counterpoise correction energy (E_{CC}) was computed through single point calculations as follows:

$$E_{CC} = E_{IL(FG^*...IL)} - E_{IL(FG...IL)} + E_{FG(FG...IL^*)} - E_{FG(FG...IL)} \qquad \text{(Equation 3)}$$

In this equation, $E_{IL(FG...IL)}$ and $E_{FG(FG...IL)}$ terms are the energy of the isolated IL molecule and FG surface respectively in the same relaxed geometry as determined for the FG…IL complexes. In addition, $E_{IL(FG^*...IL)}$ / $E_{FG(FG...IL^*)}$ term is the energy of the IL molecule/FG surface in the relaxed geometry of FG…IL complex replacing atoms of the FG surface / IL molecule with ghost atoms.

The ChelpG charge (charges from electrostatic potentials using a grid-based method) analysis [47], based on the representation of the electrostatic potential determined at the van der Waals surface, was carried out to quantify the charge transfer between FG model and ILs at the M06-2X/cc-pVDZ level. The optical properties of the studied systems were calculated using TD-DFT at the M06-2X/cc-pVDZ level of theory. All the calculations were carried out using the Gaussian 09 suite of programs [48]. The quantum theory of atoms in molecules (QTAIM) [49] was used to characterize the nature and strength of interaction between FG model and ILs. The wave functions generated at the M06-2X/cc-pVDZ level were used for QTAIM analysis using AIM2000 package [50]. The sensitivity of FG model toward adsorption of ILs was further analyzed by density of states (DOSs) calculations using GaussSum [51]. Finally, the global molecular descriptors such as HOMO-LUMO energy gap (E_g), Fermi energy level (E_{FL}), work function (WF), electronic chemical potential (μ), chemical hardness (η), global softness (S) and electrophilicity index (ω) were calculated for the FG model and then the effect of IL adsorption on these parameters was investigated.

3. Results and Discussions

3.1. Structure, stability and the nature of intermolecular interactions in FG…IL complexes

To find the most stable geometries of ionic liquids (ILs), we used the method described previously in the literature [39-40,52-57]. In this method, the conformational space around the most stable geometry of $[Bmim]^+$ and $[Btma]^+$ cations are divided into several regions and then the most stable geometry of $[BF_4]^-$, $[PF_6]^-$, and $[Tf_2N]^-$ anions was identified for each of these regions (see supporting information Scheme S1). There were also several other energetically low-lying sub-configurations in each region, which involved different orientations of the anion with respect to the cation. For example, the $[BF_4]^-$ anion could interact with the cations through one, two, or three of its fluorine atoms. Finally, all of these prepared initial structures were fully optimized at the M06-2X/cc-pVDZ level of theory and then the most stable geometries of ILs were determined and are provided as Figure 1.

In the next step, the possible adsorption structures of these ionic liquids on the FG surface were investigated and then the most stable geometries of FG…IL complexes were determined. These ILs were allowed to approach the FG surface through all possible binding modes, including *via* the imidazolium ring, the methyl or butyl groups of $[Bmim]^+$ and $[Btma]^+$ cations, or the heteroatoms (N, O, and F atoms) of the $[BF_4]^-$, $[PF_6]^-$ and $[Tf_2N]^-$ anions. Possible adsorption modes of the ILs on the FG surface were estimated according to the methodology used and described in our previous studies [39-40]. To better understand the possible adsorption configurations of ILs on the FG surface, the initial structures for adsorption of the $[Bmim][BF_4]$ ionic liquid on the FG surface are shown in Figure S1. In this method, the ILs are placed on the FG surface at a vertical distance of 2.7 Å using a variety of possible initial orientation. Based on this method, 60 different initial structures were built and then optimized at the M06-2X/cc-pVDZ level of theory. Then, the optimized FG…IL complexes were arranged according to their energy from the lowest energy to the highest energy. Finally, the lowest energy geometries for each FG…IL complex were identified and introduced as the most stable complexes in Figure 2.

It is worth mentioning that the nature of interaction of these ILs with the FG surface is different from those of the graphene surface-IL complexes reported in our previous work [40]. It is well established that the interaction of ILs with graphene surface is governed by several cooperative non-covalent interactions such as π···π, C-H···π and X···π (X = N, O and F atoms from anions) [40]. Lacking graphene's π-system, the interactions with FG are certainly expected to be different

and are comprised of a series of weak interactions, including C-H···F-C, S=O···F-C, C-F···F-C and C (IL site)···F-C (FG surface) interactions. To illustrate the role of these non-covalent interactions (NCIs) on IL adsorption, the reduced density gradient (RDG) isosurface (at 0.5 a.u.) and the scatter plot of RDG versus sign(λ_2)ρ for adsorption of ILs on the FG surface was generated using the NCI technique (Figure S2). These confirmed that the observed van der Waals (vdW) interactions between ILs and FG surface arise mainly from the cooperative C-H···F-C, S=O···F-C, C-F···F-C and C (IL site)···F-C (FG surface) interactions.

To obtain more insight into the exact nature and strength of these key interactions, QTAIM analysis [49] was used. The QTAIM parameters at the bond critical points (BCPs) and ring critical points (RCPs) formed between ILs and FG surface are summarized in Tables S1 and S2, respectively. In addition, the representation of the paths of the BCPs is shown in Figure S3. The accumulation of electron density (ρ(r)) at the bond critical points (BCPs) connecting the atoms is used to describe the strength of the bond [58]. For covalent bonds, the ρ(r) at the BCPs is of the order 0.1 a.u., while for the non-covalent interactions, it is at least one order of magnitude lower (≤ 0.01 a.u.). Accordingly, as seen from Table S1, the ρ(r) values at the BCPs between ILs and FG surface are about 0.01 a.u. or less, which confirms the non-covalent character of these interactions, these energies, between both anionic and cationic species with the FG, summarized in Table 1. Comparing the FG…[Bmim][Y] with the FG…[Btma][Y] (Y = BF_4^-, PF_6^-, and Tf_2N^-) complexes shows some differences in behavior. For FG…[Bmim][Y], the ∑ρ(r) values for the cation are greater than those of anion in all cases; while in the case of FG…[Btma][Y] complexes, ∑ρ(r) values for interaction of the anions are greater than that of the $[Btma]^+$ cation except in the case of the $[Tf_2N]^-$ anion. This discrepancy is due to the stronger affinity of the $[Bmim]^+$ cation than the $[Btma]^+$ cation for the FG surface. Independent of the identity of the cation, the anions show the same order of affinity ($[PF_6]^-$> $[BF_4]^-$> $[Tf_2N]^-$).

The Laplacian of the electron density ($\nabla^2\rho(r)$) provides further valuable information about the bonding interaction. A positive value of $\nabla^2\rho(r)$ indicates a local depletion of electron density at the BCP, suggesting a closed shell interaction. A negative value of $\nabla^2\rho(r)$, however, indicates that the bond is covalent. As seen in Table S1, the sign of $\nabla^2\rho(r)$ at the BCPs between ILs and FG surface is positive further demonstrating the non-covalent nature of these interactions. In addition, to gain further insight into the nature of interactions, the H(r) values were calculated using the sum

of kinetic energy density G(r) and potential energy density V(r) at the BCPs between the ILs and the FG surface [59-61]. The positive sign of H(r) (Table S1) at the BCPs also supports the non-covalent nature of the interactions between ILs and FG surface.

The most stable identified geometries of ionic liquids are provided as Figure 1. In these structures, the C-H bonds in the $[Bmim]^+$ and $[Btma]^+$ cations interact with the N, O and F atoms of the $[BF_4]^-$, $[PF_6]^-$ and $[Tf_2N]^-$ anions through intermolecular hydrogen bonds. The bond lengths of the C-H…X (X = N, O and F) hydrogen bonds are in the range of 2.061 Å to 2.935 Å in the [Bmim][Y] (Y = BF_4^-, PF_6^-, and Tf_2N^-) ionic liquids and 1.997 Å to 3.255 Å in the [Btma][Y] (Y = BF_4^-, PF_6^-, and Tf_2N^-) systems. It is worth noting that these hydrogen bond interactions are not dramatically affected upon adsorption. Small variations in the bond lengths of hydrogen bond interactions can be due to competing weak non-covalent interactions between the ILs and the FG surface.

The closest distance between the ILs and the nearest fluorine (F) atom of the FG surface in the FG…[Bmim][Y] and FG…[Btma][Y] (Y = BF_4^-, PF_6^-, and Tf_2N^-) complexes are related to the strength of the C-H···F-C interactions and range from 2.294 Å to 2.528 Å for Bmim and from 2.191 Å to 2.310 Å for Btma respectively. To illustrate the interactions between the ILs and the FG surface, the paths of the BCPs formed between them are presented in Figure S3. A view to the paths of the BCPs in the FG[Bmim][Tf_2N] and FG[Btma][Tf_2N] complexes indicates that the adsorption of these ILs on the FG surface mainly occurs through interaction of the C-H bonds of the $[Bmim]^+$ and $[Btma]^+$ cations, and the O and F atoms of $[Tf_2N]^-$ anion, with the F atoms of the FG surface.

The orientation of the ionic liquids also differs between these systems. As seen in Figure 2, the $[Bmim]^+$ cation in the FG…[Bmim][Y] (Y = BF_4^- and PF_6^-) complexes adopts a similar orientation with respect to the FG surface. In both complexes, the imidazolium ring is parallel to the FG surface but tilts itself slightly so that the methylated imidazolium nitrogen (N) atom is nearer to the FG surface than the butylated nitrogen. In addition, $[BF_4]^-$ and $[PF_6]^-$ anions tend to interact with the FG surface through two and three of their fluorine atoms respectively. In contrast, in the FG…[Bmim][Tf_2N] complex, the $[Bmim]^+$ cation interacts with the surface through a non-classical C-H bond with the 2-position of the ring. In this complex, the butyl group shows a tendency to lie in the plane of the FG surface. Moreover, an oxygen atom of the SO_2 group and a F atom of $–CF_3$ group in the $[Tf_2N]^-$ anion interact with the FG surface. In the case of

FG…[Btma][Y] complexes, the $[Btma]^+$ cation adopts different orientations with respect to the FG surface. The $[Btma]^+$ cation in the FG…[Btma][Y] (Y = BF_4^- and Tf_2N^-) complexes tends to be oriented parallel to the FG surface, and prefers to interact through its butyl and methyl groups, while in the FG…[Btma][PF_6] complex it is perpendicular to the FG surface and binds using two of its methyl groups. The $[BF_4]^-$ and $[PF_6]^-$ anions interact with the FG surface through three of their F atoms, whereas the $[Tf_2N]^-$ anion interacts with the FG surface via two F atoms of the –CF_3 group and one O atom of –SO_2 group.

In order to evaluate and compare the strength of interaction of the different ILs with the FG surface, the binding energy (ΔE_b) values were calculated at the M06-2X/cc-pVDZ level according to equation 1. These range from -1.68 to -2.31 kcal/mol (Table 1) and represent only very modest affinities. The ΔE_b values for adsorption of [Bmim][Y] (Y = BF_4^-, PF_6^-, and Tf_2N^-) ILs on the FG surface is higher than those of [Btma][Y] (Y = BF_4^-, PF_6^-, and Tf_2N^-) ILs. However, the rank order of adsorption of [Bmim][Y] and [Btma][Y] (Y = BF_4^-, PF_6^-, and Tf_2N^-) ILs on the FG surface is similar and as follows: [Y][Tf_2N] > [Y][PF_6] > [Y][BF_4] (Y = $Bmim^+$ and $Btma^+$). We also compared the trend of these ILs for adsorption on the FG surface with respect to graphene and hexagonal boron-nitride surfaces. The binding energies calculated at the M06-2X/cc-pVDZ level for adsorption of these ILs on the graphene and hexagonal boron-nitride sheets are reproduced from our previous studies [39-40] and are summarized in Figure 3 for comparison purposes. The adsorption of ILs to the surfaces, regardless of IL identity, is generally found to be in order of graphene > hexagonal boron-nitride > fluorographene, indicating that fluorinating the graphene surface strongly decreases the binding energy of ILs. This is as expected as FG lacks the π system and the strong potential dipole interactions of graphene and boron nitride.

The charge analysis estimated using the ChelpG method revealed that upon adsorption of ILs, the charge of FG surface changes significantly (Table 1). According to this analysis, the negative sign of induced charge on the FG surface ($\Delta q_{(Surface)}$) indicates that the charge is transferred from the ILs to the FG surface with the exception of FG…[Btma][PF_6] complex. A comparison between the amount of charge transfer in the FG…IL complexes and that in the graphene…IL and hexagonal boron-nitride…IL complexes [39-40] shows that the amount of charge transfer in the FG…[Bmim][Y] (Y = BF_4^-, PF_6^-, and Tf_2N^-) complexes is greater than that in the graphene (hexagonal boron-nitride)…[Bmim][Y] complexes. In addition, the amount of charge transfer in the FG…[Btma][Y] (Y = BF_4^-, PF_6^-, and Tf_2N^-) complexes doesn't show a clear trend in

comparison to graphene (hexagonal boron-nitride)…[Btma][Y] complexes. This observation indicates that the lack of a π system in FG surface can be a significant factor for determining the degree of charge transfer.

3.2. HOMO−LUMO energy gap, density of states (DOSs) and global molecular descriptors

The interaction character and charge transfer between ILs and the FG surface may affect the electronic structure of the FG surface. To probe this, density of states (DOSs) were then calculated for the FG surface and all the complexes involved in this study (see Figure S4 in the Supporting Information for details of the calculated DOSs). The predicted DOSs showed that IL adsorption leads to small changes in the DOS pattern of FG surface.

The HOMO energy level of the FG surface is destabilized and the LUMO energy level is stabilized after adsorption of ILs except in the case of adsorption of ILs containing $[BF_4]^-$ anion (Figure S4). The variations in the energy of the frontier molecular orbitals leads to change in the HOMO-LUMO energy gap (E_g) of different FG…IL complexes (Table 1). The calculated E_g values show that the adsorption of ILs on the FG surface decreases the HOMO-LUMO energy gap of FG surface, which leads to an increase in the number of electrons in the conduction band and in turn results in enhanced conductivity.

The calculated HOMO-LUMO energy gap is a main feature in determining the electrical conductivity (σ) of a material because the energy required for removing an electron from the outermost shell is equivalent to E_g value. The classic relationship is described by the following equation [55[59]:

$$\sigma \propto \exp\left(\frac{-E_g}{2k_B T}\right) \qquad \text{(Equation 4)}$$

where E_g is the HOMO-LUMO energy gap, k_B is the Boltzmann constant, and T is the temperature in Kelvin. According to this equation, a larger HOMO-LUMO energy gap at a given temperature leads to less electrical conductivity and vice versa. Comparing the E_g values of the FG…IL complexes shows that the electrical conductivities of FG…[Bmim][Y] (Y = BF_4^-, PF_6^-, and Tf_2N^-) complexes are predicted to be greater than FG…[Btma][Y] complexes. The amount of decrease in the HOMO-LUMO energy gap of FG surface with adsorption of ILs is provided as ΔE_g in Table 1. The adsorption of [Bmim][Y] (Y = BF_4^-, PF_6^-, and Tf_2N^-) ILs decreases the HOMO-LUMO energy gap of FG surface more than the adsorption of [Btma][Y] (Y = BF_4^-, PF_6^-,

and Tf_2N^-) ILs. The smallest decrease in the HOMO-LUMO energy gap of the FG surface is observed for the adsorption of ILs containing $[BF_4]^-$ anion and the greatest decreases are achieved by adsorption of ILs containing $[Tf_2N]^-$ anion; this is in complete agreement with the observed trend of IL adsorption with FG surfaces: the greater the binding energy, the greater is the decrease in the E_g of FG surface (more negative values of ΔE_g) upon IL adsorption. The Fermi energy level of the FG surface rises upon adsorption of ILs. The most significant shifts in the Fermi energy level are achieved via adsorption of [Bmim][Tf_2N] and [Btma][Tf_2N] ILs.

The minimum energy required to remove an electron from the Fermi level to the vacuum level of a surface is defined as the Work Function (WF) of the surface and is calculated according to the following equation:

$$WF = E_{inf} - E_{FL} \qquad \text{(Equation 5)}$$

where E_{inf} is the electrostatic potential at infinity (vacuum level),a nd E_{FL} is the Fermi level energy of the system [5559]. E_{inf} is assumed to be approximately zero as any error does not have a significant impact on the analysis of the relative values of the WF of the surface and its complexes. The canonical assumption for the position of Fermi level (at T = 0 K) for any given molecule is the exact center of the energy gap (E_g) [59]. This is because the energy of the center of the E_g is the chemical potential of the system (μ). The chemical potential of a free gas of electrons is equal to its Fermi level so the Fermi level is equal to the value at the center of the E_g [62]. The work function changes (ΔWF) were calculated by subtracting the work function of the FG surface from that of the corresponding FG…IL system. The greatest decrease in WF was observed for the adsorption of [Bmim][Tf_2N] and [Btma][Tf_2N] ILs. Finally, a negative ΔWF value (Table 1) may arise from a donation of charge from the IL to the FG surface, which correlates with an increase in the electrical conductivity of FG surface upon exposure to the IL as has been previously shown. . According to our results, the E_F value of FG surface increases upon IL adsorption. Therefore, the potential barrier for electron emission from the FG surface is decreased due to the reduction in the work function. Thus, the emission from the FG surface will be facilitated by adsorption of ILs. A significant improvement in the field emission properties of the FG surface is observed when [Bmim][Y] (Y = BF_4^-, PF_6^-, and Tf_2N^-) ILs are adsorbed on the FG surface.

To better understand the effect of IL adsorption on the electronic properties of the FG surface, the properties such as chemical potential (μ), chemical hardness (η), global softness (S), and

electrophilicity index (ω) [63-65] were also calculated for FG surface (Figure 4, Table S3) and the different FG…IL complexes according to Koopmans' theorem [66].

The μ value of the FG surface increases with improved adsorption of ILs; the μ value of the [Bmim] complexes is greater than for the [Btma] ILs. In addition, the predicted chemical hardness (η) of FG surface decreases with greater adsorption of ILs. To explain the observed reactivity trends, we could say that a high HOMO-LUMO energy gap (E_g) indicates greater stability and lower reactivity of the chemical system and a soft molecule with a small energy gap will be more polarizable than hard molecules with a large energy gap. According to this criterion, the FG…[Btma][Y] complexes are predicted to be harder (more η value) and have lower reactivity than FG…[Bmim][Y] complexes due to their higher E_g values. In addition, the relative electrophilic nature of a molecule is evaluated using a global molecular descriptor known as electrophilicity index (ω). This descriptor measures the stabilization in energy when the system gains an additional electronic charge (ΔN) from the environment. A good electrophile is determined by a high value of μ and a low value of η. Our results in Figure 4 show that the ω value of FG surface generally decreases upon adsorption of ILs and the FG…[Btma][Y] complexes are better electrophiles than FG…[Bmim][Y] complexes.

3.3. Optical properties

UV–vis spectroscopy has proven to be an effective optical characterization tool for understanding the electronic structure of semiconductor materials [67]. Fluorographene has drawn growing attention due to its hydrophobic surface, sp^3 architecture, and outstanding properties [68]. Wang and co-workers have shown that the fluorination of graphene leads to a blue shift for the characteristic $\pi \rightarrow \pi^*$ electron transition of the C=C from 269 nm to 251 nm and 247 nm [16], demonstrating that the bandgap is opened by the introduction of C-F covalent bonds in graphene. They also observed that additional new peaks arise as the extent of fluorination increases. Mazánek and co-workers have also synthesized a series of fluorinated graphene surfaces with various degrees of fluorine substitution [69]. They found that the position of absorption peaks is dependent on the extent of fluorination.

In this study, we computationally investigated the UV-vis spectrum of fully fluorinated graphene and analyzed the effect of ionic liquid adsorption on the optical properties of the fluorographene surface. The UV-vis absorption spectra were calculated using the TD-M06-2X/cc-

pVDZ level and shown in Figure 5. The computed wavelengths (λ), excitation energies (E), oscillator strength (f), excitation coefficients, main transitions, and different excitation states of both the fluorographene (FG) surface and FG…IL complexes were determined (Table S4). According to these calculated parameters, the UV-vis absorption spectrum of a fully-substituted FG surface shows an intense absorption band at λ = 179 nm corresponding to an electronic transition of HOMO-1 → LUMO, which corresponds to electronic transitions from nonbonding electrons of a F atom to the antibonding orbital of C-F ($n \rightarrow \sigma^*_{(C\text{-}F)}$) of the FG surface (Figure 5 and Table S4). The calculated spectra of FG…[Bmim][Y] and FG…[Btma][Y] (Y = BF_4^-, PF_6^-, and Tf_2N^-) complexes are similar in shape to that of the FG surface (Figure 5); the IL adsorption does not greatly change the absorption spectrum of FG surface and only leads to small red shifts in the absorption band at λ = 179 nm, this is to be expected as the weak FG…IL interaction would not be expected to have a significant effect on the optical behavior of the material.

The absorption spectra of the FG…[Bmim][Y] (Y = BF_4^- and PF_6^-) complexes are characterized by two absorption bands, except while those of the FG…[Bmim][Tf_2N^-] and all the FG…[Btma][Y] (Y = BF_4^- and PF_6^-) complexes show only one absorption band. The absorption spectra of the FG…[Bmim][BF_4] and FG…[Bmim][PF_6] complexes are characterized by two absorption bands at 180 nm and 201 nm for FG…[Bmim][BF_4] complex and slightly more red shift peaks of 181 nm and 205 nm for FG…[Bmim][PF_6]. In these complexes, the stronger absorption bands (λ = 180.3 nm and 180.7 nm) are related to HOMO-5 → LUMO electronic transitions, while weaker absorption bands (λ = 201 nm and 205 nm) are associated with HOMO → LUMO transitions. The only absorption band observed for the FG…[Bmim][Tf_2N] complex is located at 180.0 nm and is associated with the HOMO-13 → LUMO electronic transition. The main transition configurations for the FG…[Btma][Y] complexes are shown in Figure 5. A comparison between the strength and red-shift of the absorption bands of these complexes indicates that the FG…[Btma][PF_6] complex has a weaker absorption band (E = 6.83 eV) with a higher wavelength (181.4) in comparison to either the FG…[Btma][BF_4] or the FG…[Btma][Tf_2N] complexes. The absorption bands in the FG…[Btma][BF_4], FG…[Btma][PF_6] and FG…[Btma][Tf_2N] complexes are associated with the HOMO-2→LUMO, HOMO-3→LUMO and HOMO-12→LUMO transitions, respectively.

4. Conclusions

The adsorption of [Bmim][Y] and [Btma][Y] (Y = BF_4^-, PF_6^-, and Tf_2N^-) ionic liquids (ILs) on the fluorographene (FG) surface and the corresponding changes in the FG electronic structure have been investigated using DFT based methods. Binding energy (ΔE_b) calculations show that the fluorination of graphene surface significantly decreases the adsorption strength of ILs with respect to graphene and hexagonal boron nitride surfaces such that for almost any IL, the binding affinities follow a predictable trend: $\Delta E_{b\ (Graphene\cdots IL)} > \Delta E_{b\ (Hexagonal\ boron\text{-}nitride\cdots IL)} > \Delta E_{b\ (Fluorographene\cdots IL)}$. The low binding energy of ILs in the FG…IL complexes arises due to the presence of a series of weak non-covalent interactions, including C-H···F-C, S=O···F-C, C-F···F-C and C (from IL)···F-C (from FG surface), between ILs and FG surface, as highlighted by non-covalent interaction (NCI) plots and further confirmed by QTAIM analysis. Furthermore, a comparison between the adsorption strength of ILs on the FG surface shows that [Bmim][Y] ILs show higher affinity for FG than their [Btma][Y] counterparts. The rank order of adsorption is also dependent on the anion as follows: [X][Tf_2N] > [X][PF_6] > [X][BF_4] (X = $Bmim^+$ and $Btma^+$). The degree of charge transfer from the ILs to the FG surface is evident from the ChelpG charge analysis. Density of states (DOSs) calculations indicate that the presence of non-covalent interactions and charge transfer leads to variations of the HOMO and LUMO energy levels of the FG surface. The HOMO-LUMO energy gap (E_g) of the FG surface significantly decreases, meaning leading to an enhancement in electrical conductivity upon adsorption of ILs. The greater the amount of binding energy, the greater the decrease in the E_g value of the FG surface with adsorption of ILs. According to our results, the FG…[Btma][Y] complexes have bigger E_g values, higher η values and lower reactivities than the FG…[Bmim][Y] complexes. Electronic property calculations show that the adsorption of ILs increases the μ value of FG surface, while the η and ω values of FG surface decrease upon adsorption of ILs. Finally, a comparison of the UV-vis absorption spectra of FG and FG…IL complexes shows that IL adsorption leads to small red shifts in the λ = 179.4 nm absorption band of the FG spectrum. The insights obtained from this current study will be useful in future optoelectronic device design using fluorographene semiconductors.

Acknowledgement

SMT and JFT would like to thank the University of Windsor for providing funding for this project. This work was made possible by the facilities of the Shared Hierarchical Academic Research Computing Network (SHARCNET: www.sharcnet.ca) and computing resources. MS-F. would like to thank Birjand University of Technology for financial support for this work. The authors declare that they have no competing financial interest.

Supporting Information

This material contains molecular structures of cations and anions forming ionic liquids, the initial structures for adsorption of [Bmim][BF_4] ionic liquid on the FG surface, the results of non-covalent interaction (NCI) plots of the FG…IL complexes, QTAIM analysis, the paths of the bond critical points (BCPs) formed between ILs and FG surface, density of states (DOSs) of FG surface and FG…IL complexes, global molecular descriptors, vertical excitation process of FG surface and FG…IL complexes and cartesian coordinates of all optimized structures used in this work.

References

[1] S.S. Varghese, S. Lonkar, K.K. Singh, S. Swaminathan, A. Abdala, Recent advances in graphene based gas sensors, Sens. Actuators, B, 218 (2015) 160-183.

[2] R. Raccichini, A. Varzi, S. Passerini and B. Scrosati, The role of graphene for electrochemical energy storage, Nat. Mater., 14 (2014) 271-279.

[3] S.J. Heerema and C. Dekker, Graphene nanodevices for DNA sequencing, Nat. Nanotechnol., 11 (2016) 127-136.

[4] J. Rafiee, X. Mi, H. Gullapalli, A.V. Thomas, F. Yavari, Y. Shi, P.M. Ajayan and N.A. Koratkar, Wetting transparency of graphene, Nat. Mater., 11 (2012) 217-222.

[5] S. Stankovich, D.A. Dikin, G.H.B. Dommett, K.M. Kohlhaas, E.J. Zimney, E.A. Stach, R.D. Piner, S.T. Nguyen and R.S. Ruoff, Graphene-based composite materials, Nature, 442 (2006) 282-286.

[6] N. Kumar, J. D. Sharma and P.K. Ahluwalia, Pramana, First-principle study of nanostructures of functionalized graphene, Pramana – J. Phys., 82 (2014) 1103-1117.

[7] G. Akilas, V. Otyepk, M. Bourlinos, A.B. Chandra, V. Kim, N. Kemp, K.C. Hobza, P. Zboril, R. Zboril, K.S. Kim, Functionalization of graphene: Covalent and non-covalent approaches, derivatives and applications, Chem. Rev, 112 (2012) 6156 -6214.

[8] L.I. Alexander, Graphene-based and graphene-like materials, Russ. Chem. Rev., 81 (2012) 571-605.

[9] J.E. Johns, M.C. Hersam, Atomic covalent functionalization of graphene, Acc. Chem. Res., 46 (2013) 46 77-86.

[10] E. Bordes, J. Szala-Bilnik and A.A.H. Padua, Exfoliation of graphene and fluorographene in molecular and ionic liquids, Faraday Discuss., 206 (2018) 61-75.

[11] R.R. Nair, W. Ren, R. Jalil, I. Riaz, V.G. Kravets, L. Britnell, P. Blake, F. Schedin, A.S. Mayorov, S. Yuan, M.I. Katsnelson, H.M. Cheng, W. Strupinski, L.G. Bulusheva, A.V. Okotrub,

I.V. Grigorieva, A.N. Grigorenko, K.S. Novoselov and A.K. Geim, Fluorographene: A two-dimensional counterpart of teflon, Small, 6 (2010) 2877-2884.

[12] D.D. Chronopoulos, A. Bakandritsos, M. Pykal, R. Zbořil and M. Otyepka, Chemistry, properties, and applications of fluorographene, Appl. Mater. Today, 9 (2017) 60-70.

[13] P. Gong, Z. Wang, Z. Li, Y. Mi, J. Sun, L. Niu, H. Wang, J. Wang and S. Yang, Photochemical synthesis of fluorinated graphene via a simultaneous fluorination and reduction route, RSC Adv., 3 (2013) 6327-6330.

[14] S.B. Bon, L. Valentini, R. Verdejo, J.L. Garcia Fierro, L. Peponi, M.A. Lopez-Manchado, J.M. Kenny, Plasma fluorination of chemically derived graphene sheets and subsequent modification with butylamine, Chem. Mater, 21 (2009) 3433-3438.

[15] K. Samanta, S. Some, Y. Kim, Y. Yoon, M. Min, S.M. Lee, Y. Park, H. Lee, Highly hydrophilic and insulating fluorinated reduced graphene oxide, Chem. Commun, 49 (2013) 8991-8993.

[16] Z. Wang, J. Wang, Z. Li, P. Gong, X. Liu, L. Zhang, J. Ren, H. Wang, S. Yang, Synthesis of fluorinated graphene with tunable degree of fluorination, Carbon, 50 (2012) 5403-5410.

[17] S.K. Yadav, J.H. Lee, H. Park, S.M. Hong, T.H. Han, C.M. Koo, Facile and ecofriendly fluorination of graphene oxide, Bull. Korean Chem. Soc., 35 (2014) 2139-2142.

[18] F.G. Zhao, G. Zhao, X.H. Liu, C.W. Ge, J.T. Wang, B.L. Li, Q.G. Wang, W.S. Li and Q.Y. Chen, Fluorinated graphene: Facile solution preparation and tailorable properties by fluorine-content tuning, J. Mater. Chem. A, 2 (2014) 8782-8789.

[19] J.T. Robinson, J.S. Burgess, C.E. Junkermeier, S.C. Badescu, T.L. Reinecke, F.K. Perkins, M.K. Zalalutdniov, J.W. Baldwin, J.C. Culbertson, P.E. Sheehan and E.S. Snow, Properties of fluorinated graphene films, Nano Lett., 10 (2010) 3001–3005.

[20] R. Zborˇil, F. Karlicky´, A.B. Bourlinos, T.A. Steriotis, A.K. Stubos, V. Georgakilas, K. Sˇafárˇová, D. Jancˇík, C. Trapalis and M. Otyepka, Graphene fluoride: A stable stoichiometric graphene derivative and its chemical conversion to graphene, small 6 (2010) 2885–2891.

[21] S.H. Cheng, K. Zou, F. Okino, H.R. Gutierrez, A. Gupta, N. Shen, P.C. Eklund, J.O. Sofo and J. Zhu, Reversible fluorination of graphene: Evidence of a two-dimensional wide bandgap semiconductor, Phys. Rev. B, 81 (2010) 205435.

[22] H. Yang, M. Chen, H. Zhou, C. Qiu, L. Hu, F. Yu, W. Chu, S. Sun and L. Sun, Preferential and reversible fluorination of monolayer graphene, J. Phys. Chem. C, 115 (2011) 16844–16848.

[23] V. Nicolosi, M. Chhowalla, M.G. Kanatzidis, M.S. Strano, and J.N. Coleman, Liquid exfoliation of layered materials, Science, 340 (2013) 1226419.

[24] H. Chang, J. Cheng, X. Liu, J. Gao, M. Li, J. Li, X. Tao, F. Ding and Z. Zheng, Facile synthesis of wide-bandgap fluorinated graphene semiconductors, Chem. Eur. J., 17 (2011) 8896-8903.
[25] F. Soavi, S. Monaco and M. Mastragostino, Catalyst-free porous carbon cathode and ionic liquid for high efficiency, rechargeable Li/O_2 battery, J. Power Sources, 224 (2013) 115-119.
[26] H. Kurig, M. Vestli, K. Tonurist, A. Janes, E. Lust, Influence of room temperature ionic liquid anion chemical composition and electrical charge delocalization on the supercapacitor properties, J. Electrochem. Soc., 159 (2012) 944-951.
[27] Z. Lei, Z. Liu, H. Wang, X. Sun, L. Lu and X.S. Zhao, A high-energy-density supercapacitor with graphene–CMK-5 as the electrode and ionic liquid as the electrolyte, J. Mater. Chem. A, 1 (2013) 2313-2321.
[28] P. Simon and Y. Gogotsi, Materials for electrochemical capacitors, Nat. Mater., 7 (2008) 845-854.
[29] T. Fujimoto and K. Awaga, Electric-double-layer field-effect transistors with ionic liquids, Phys. Chem. Chem. Phys., 15 (2013) 8983-9006.
[30] M. Vijayakumar, B. Schwenzer, V. Shutthanandan, J.Z. Hu, J. Liu and I.A. Aksay, Elucidating graphene−ionic liquid interfacial region: A combined experimental and computational study, Nano Energy, 3 (2014) 152−158.
[31] X. Zhou, T. Wu, K. Ding, B. Hu, M. Hou and B. Han, Dispersion of graphene sheets in ionic liquid [bmim][PF_6] stabilized by an ionic liquid polymer, Chem. Commun., 46 (2010) 386−388.
[32] A.S. Pensado, F. Malberg, M.F. Costa Gomes, A.A.H. Padua, J. Fernandez and B. Kirchner, Interactions and structure of ionic liquids on graphene and carbon nanotubes surfaces, RSC Adv., 4 (2014) 18017−18024.
[33] S. Aparicio and M. Atilhan, Molecular dynamics study of carbon nanostructures in N-methylpiperazinium lactate ionic liquid, J. Phys. Chem. C, 117 (2013) 22046−22059.
[34] G. García, M. Atilhan and S. Aparicio, Adsorption of choline benzoate ionic liquid on graphene, silicene, germanene and boron-nitride nanosheets: A DFT perspective, Phys. Chem. Chem. Phys., 17 (2015) 16315-16326.
[35] G. García, M. Atilhan and S. Aparicio, Flavonols on graphene: A DFT insight, Theor Chem Acc, 134 (2015) 57.
[36] C. Herrera, G. García, M. Atilhan and S. Aparicio, Nanowetting of graphene by ionic liquid droplets, J. Phys. Chem. C, 119 (2015) 24529–24537.

[37] M. Atilhan and S. Aparicio, Folding of graphene nanostructures driven by ionic liquids nanodroplets, J. Phys. Chem. C, 118 (2014) 21081−21091.
[38] F. Karlicky, E. Otyepkova, R. Lo, M. Pitonak, P. Jurecka, M. Pykal, P. Hobza, M. Otyepka, Adsorption of organic molecules to van der Waals materials: Comparison of fluorographene and fluorographite with graphene and graphite, J. Chem. Theory Comput., 13 (2017) 1328-1340.
[39] M. Shakourian-Fard, G. Kamath and Z. Jamshidi, Trends in physisorption of ionic liquids on boron-nitride sheets, J. Phys. Chem. C, 118 (2014) 26003-26016.
[40] M. Shakourian-Fard, Z. Jamshidi, A. Bayat and G. Kamath, Meta-hybrid density functional theory study of adsorption of imidazolium- and ammonium-based ionic liquids on graphene sheet, J. Phys. Chem. C, 119 (2015) 7095-7108.
[41] P.A. Denis, Chemical reactivity of electron-doped and hole-doped graphene, J. Phys. Chem. C, 117 (2013) 3895-3902.
[42] M. Shakourian-Fard, Z. Jamshidi and G. Kamath, Surface charge-transfer doping of graphene nanoflakes containing double-vacancy (5-8-5) and stone-wales (55-77) defects through molecular adsorption, ChemPhysChem, 17 (2016) 3289-3299.
[43] Z. Xu, B.R. Meher, D. Eustache and Y. Wang, Insight into the interaction between DNA bases and defective graphenes: Covalent or non-covalent, J. Mol. Graphics Modell., 47 (2014) 8-17.
[44] H. Roohi, K. Ghauri, R. Salehi, Non-covalent green functionalization of boron nitride nanotubes with tunable aryl alkyl ionic liquids: A quantum chemical approach, J. Mol. Liq., 243 (2017) 22-40.
[45] D. Umadevi and G.N. Sastry, Quantum mechanical study of physisorption of nucleobases on carbon materials: Graphene versus carbon nanotubes, J. Phys. Chem. Lett., 2 (2011) 1572-1576.
[46] S.F. Boys and F. Bernardi, The calculation of small molecular interactions by the differences of separate total energies. Some procedures with reduced errors, Mol. Phys., 19 (1970) 553-566.
[47] C.M. Breneman and K.B. Wiberg, Determining atom-centered monopoles from molecular electrostatic potentials. The need for high sampling density in formamide conformational analysis, J. Comput. Chem., 11 (1990) 361-373.
[48] Gaussian 09, Revision D.01, M.J. Frisch, G.W. Trucks, H.B. Schlegel, G.E. Scuseria, M.A. Robb, J.R. Cheeseman, G. Scalmani, V. Barone, B. Mennucci, G.A. Petersson, H. Nakatsuji, M. Caricato, X. Li, H.P. Hratchian, A.F. Izmaylov, J. Bloino, G. Zheng, J.L. Sonnenberg, M. Hada, M. Ehara, K. Toyota, R. Fukuda, J. Hasegawa, M. Ishida, T. Nakajima, Y. Honda, O. Kitao, H.

Nakai, T. Vreven, J.A. Montgomery, J.J.E. Peralta, F. Ogliaro, M. Bearpark, J.J. Heyd, E. Brothers, K.N. Kudin, V.N. Staroverov, R. Kobayashi, J. Normand, K. Raghavachari, A. Rendell, J.C. Burant, S.S. Iyengar, J. Tomasi, M. Cossi, N. Rega, J.M. Millam, M. Klene, J.E. Knox, J.B. Cross, V. Bakken, C. Adamo, J. Jaramillo, R. Gomperts, R.E. Stratmann, O. Yazyev, A.J. Austin, R. Cammi, C. Pomelli, J.W. Ochterski, R.L. Martin, K. Morokuma, V.G. Zakrzewski, G.A. Voth, P. Salvador, J.J. Dannenberg, S. Dapprich, A.D. Daniels, O. Farkas, J.B.
Foresman, J.V. Ortiz, J. Cioslowski, D.J. Fox, Gaussian, Inc., Wallingford, CT, 2010.

[49] R.F.W. Bader, Atom in Molecules: A Quantum Theory, Oxford University Press, Oxford, UK, 1990.

[50] AIM2000, A Program to Analyse and Visualize Atoms in Molecules, version 1 Innovative software, Bielefeld, Germany, 2002.

[51] N.M. O'Boyle, A.L. Tenderholt and K.M. Langner, cclib: A library for package-independent computational chemistry algorithms, J. Comput. Chem., 29 (2008) 839-845.

[52] M. Shakourian-Fard, A. Fattahi and A. Bayat, Ionic liquid based on α-amino acid anion and N7, N9-dimethylguaninium cation ([dMG][AA]): Theoretical study on the structure and electronic properties, J. Phys. Chem. A, 116 (2012) 5436-5444.

[53] M. Shakourian-Fard, Z. Jamshidi, A. Bayat and A. Fattahi, Structural and electronic properties of alkyl-trifluoroborate based ionic liquids: A theoretical study, J. Fluorine Chem., 153 (2013) 96-100.

[54] H.Z. Ziyaei, M. Shakourian-Fard, F.M. Vahdati, M. Raeesi, H.M. Mahmoodi and H. Behzadi, Design and synthesis of new family of ionic liquids based on 2-iminium-1,3-dithiolanes: A combined theoretical and experimental effort, J. Mol. Struct., 1056 (2013) 56-62.

[55] M. Shakourian-Fard, A. Bayat and G. Kamath, Effect of mono-vacant defects on the opto-electronic properties of ionic liquid functionalized hexagonal boron-nitride nanosheets, J. Mol. Liq., 249 (2018) 1172-1182.

[56] D. Xing, Y. Bu and X. Tan, Characterizing the properties of the N7, N9-dimethylguaninium chloride ion pairs: Prospecting for the design of a novel ionic liquid, J. Phys. Chem. A, 112 (2008) 106-116.

[57] A. Mohajeri and A. Ashrafi, Structure and electronic properties of amino acid ionic liquids, J. Phys. Chem. A, 115 (2011) 6589–6593.

[58] R. Parthasarathi, V. Subramanian, N. Sathyamurthy, Hydrogen bonding without borders: An atoms-in-molecules perspective, J. Phys. Chem. A, 110 (2006) 3349- 3351.
[59] H. Roohi, M. Jahantab, Sensitivity of perfect and stone-wales defective BNNTs toward NO molecule: A DFT/M06-2X approach, Phys. Chem. Res., 5 (2017) 167-183.
[60] S.J. Grabowski, W.A. Sokalski, E. Dyguda, J. Leszczyński, Quantitative classification of covalent and noncovalent h-bonds, J. Phys. Chem. B, 110 (2006) 6444-6446.
[61] S.J. Grabowski, What is the covalency of hydrogen bonding?, Chem. Rev., 111 (2011) 2597-2625.
[62] J. Beheshtian, A. Ahmadi Peyghan and Z. Bagheri, Detection of phosgene by Sc-doped BN nanotubes: A DFT study, Sens. Actuators, B, 171– 172 (2012) 846– 852.
[63] P. Geerlings, F. De Proft and W. Langenaeker, Conceptual density functional theory, Chem. Rev., 103 (2003) 1793-1874.
[64] R.K. Roy and S. Saha, Studies of regioselectivity of large molecular systems using DFT based reactivity descriptors, Annu. Rep. Prog. Chem., Sect. C: Phys. Chem., 106 (2010) 118-162.
[65] R.G. Parr and R.G. Pearson, Absolute hardness: Companion parameter to absolute electronegativity, J. Am. Chem. Soc., 105 (1983) 7512-7516.
[66] T. Koopman, Über die zuordnung von wellenfunktionen und eigenwerten zu den einzelnen 26 elektronen eines atoms, Physica, 1 (1933) 104-113.
[67] H. Chang, Z. Sun, Q. Yuan, F. Ding, X. Tao, F. Yan and Z. Zheng, Thin film field-effect phototransistors from bandgap-tunable, solution-processed, few-layer reduced graphene oxide films, Adv. Mater., 22 (2010) 4872-4876.
[68] M. Ren, X. Wang, C. Dong, B. Li, Y. Liu, T. Chen, P. Wu, Z. Cheng and X. Liu, Reduction and transformation of fluorinated graphene induced by ultraviolet irradiation, Phys. Chem. Chem. Phys., 17 (2015) 24056-24062.
[69] V. Mazanek, O. Jankovsky, J. Luxa, D. Sedmidubsky, Z. Janousek, F. Sembera, M. Mikulics and Z. Sofer, Tuning of fluorine content in graphene: Towards large-scale production of stoichiometric fluorographene, Nanoscale, 7 (2015) 13646-13655.

Figure Caption

Figure 1. Optimized geometries of fluorographene (FG) model and ionic liquids at M06-2X/cc-pVDZ level: (i) top view and (ii) side view.

Figure 2. The most stable geometries of FG…IL complexes optimized at the M06-2X/cc-pVDZ level. Each complex is shown from both a top-down, and side-on view for clarity.

Figure 3. Comparison of binding energies of fluorographene, graphene and hexagonal boron-nitride surfaces with ILs calculated at the M06-2X/cc-pVDZ level. The binding energies for adsorption of ILs on the graphene and hexagonal boron-nitride surfaces have been taken from our previous studies [39-40].

Figure 4. Comparison of E_g, $-\mu$, η and ω values (in eV) of FG surface and different FG…IL complexes.

Figure 5. The UV-vis absorption spectra of fluorographene surface and its complexes with ILs computed at the TD-M06-2X/cc-pVDZ level of theory.

Figure 1.

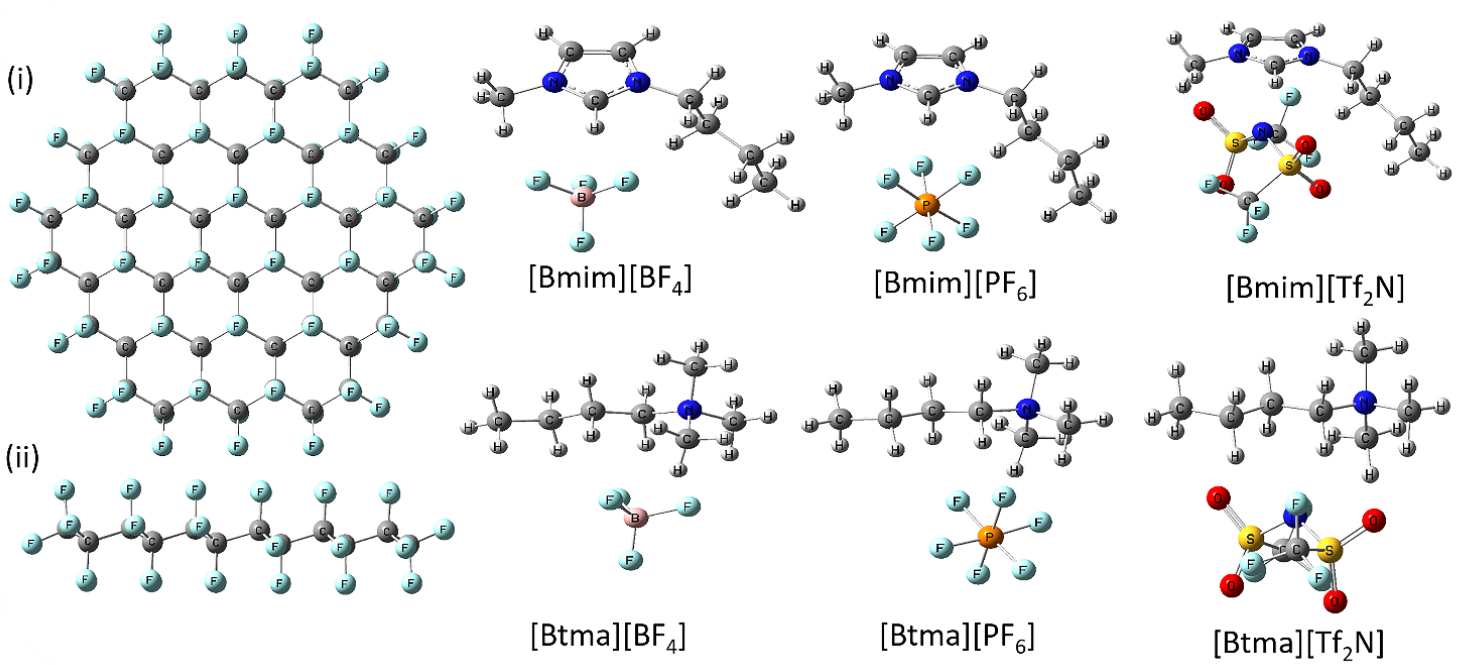

Figure 2.

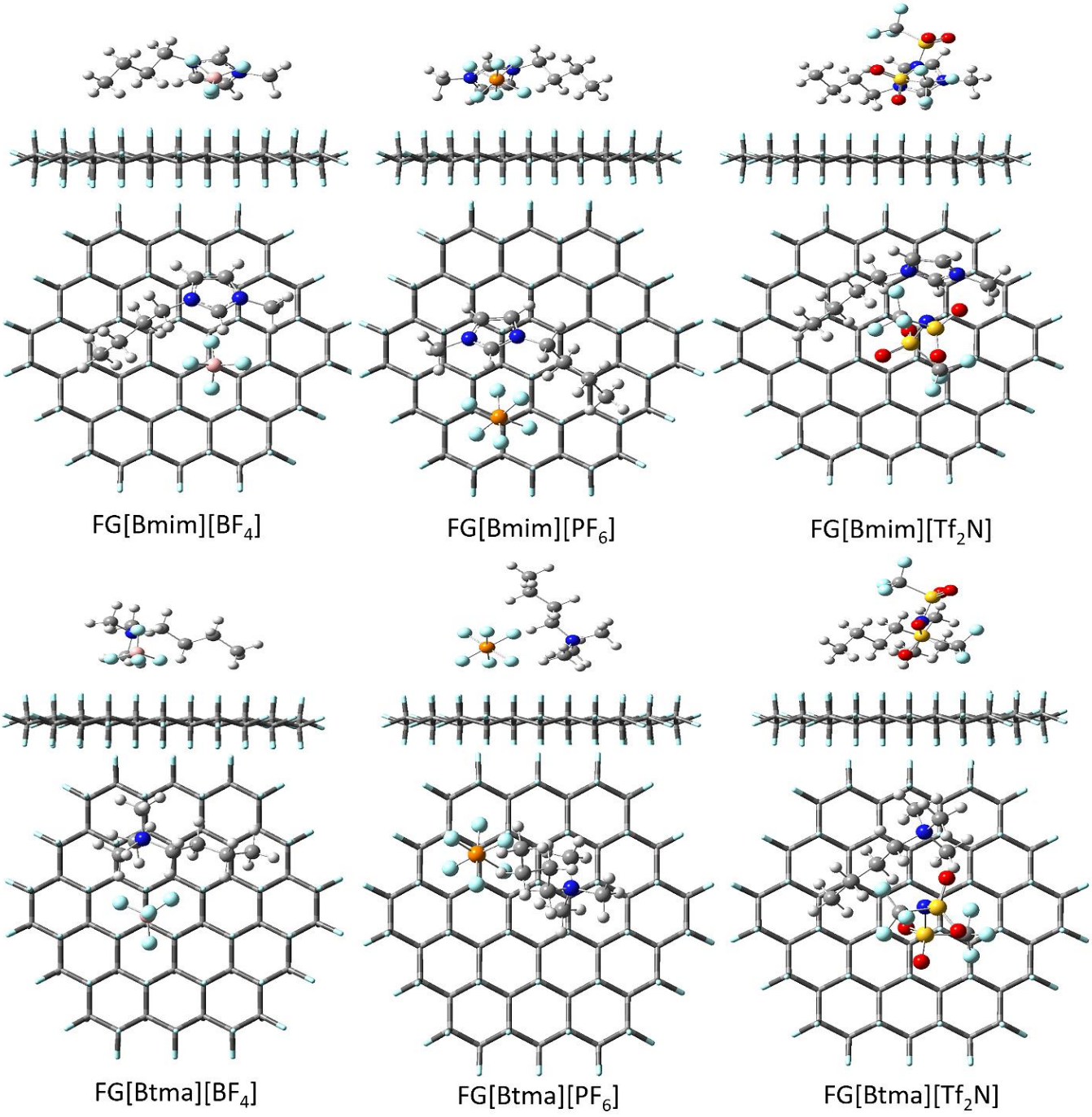
FG[Bmim][BF4]
FG[Bmim][PF6]
FG[Bmim][Tf2N]
FG[Btma][BF4]
FG[Btma][PF6]
FG[Btma][Tf2N]

Figure 3.

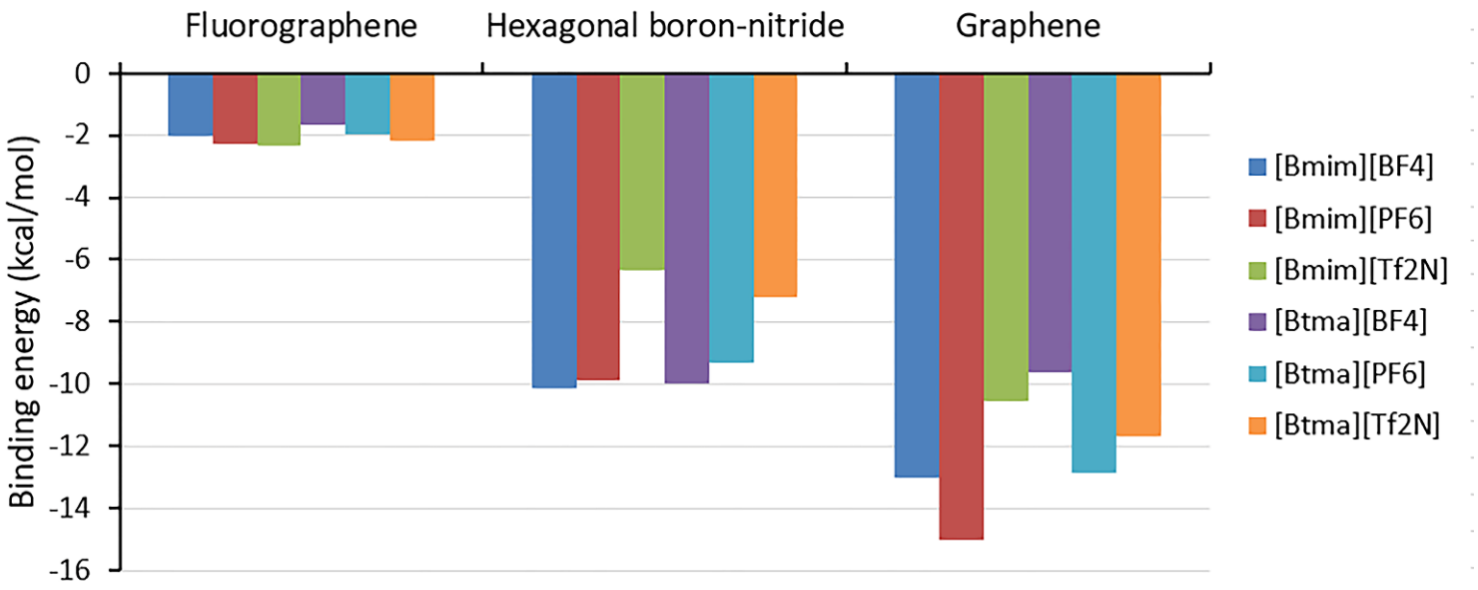
Fluorographene
Hexagonal boron-nitride
Graphene
Binding energy (kcal/mol)
0
-2
-4
-6
-8
-10
-12
-14
-16
[Bmim][BF4]
[Bmim][PF6]
[Bmim][Tf2N]
[Btma][BF4]
[Btma][PF6]
[Btma][Tf2N]

Figure 4.

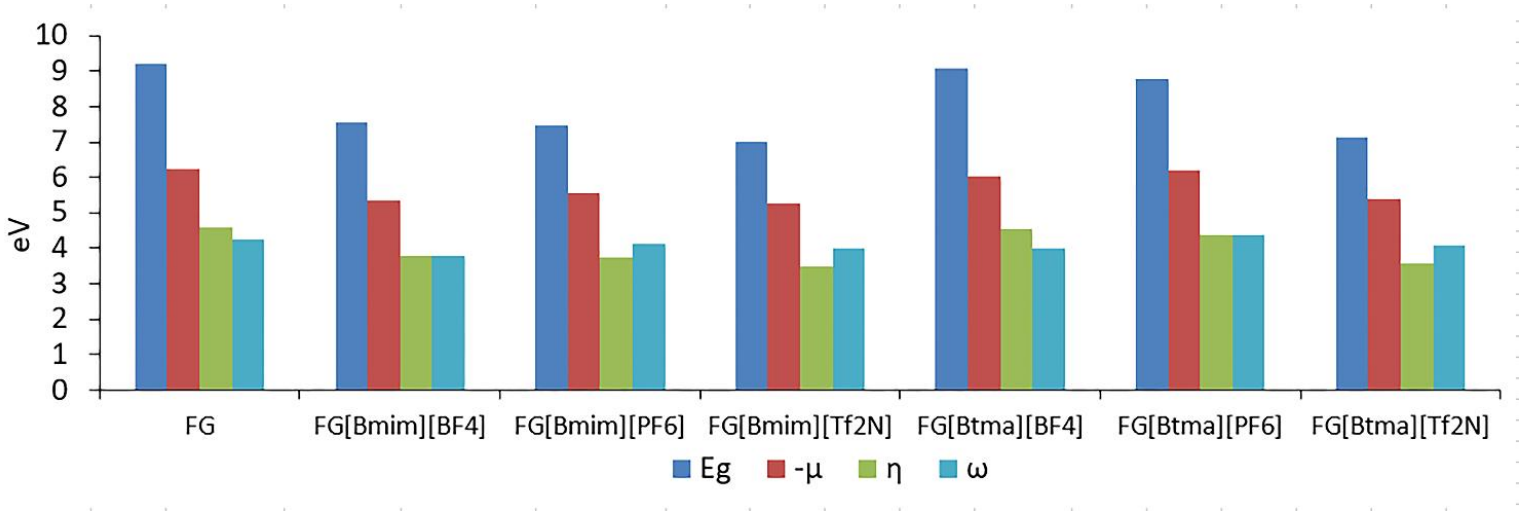
10
9
8
7
6
5
4
3
2
1
0
eV
FG
FG[Bmim][BF4]
FG[Bmim][PF6]
FG[Bmim][Tf2N]
FG[Btma][BF4]
FG[Btma][PF6]
FG[Btma][Tf2N]
Eg
-μ
η
ω

Figure 5.

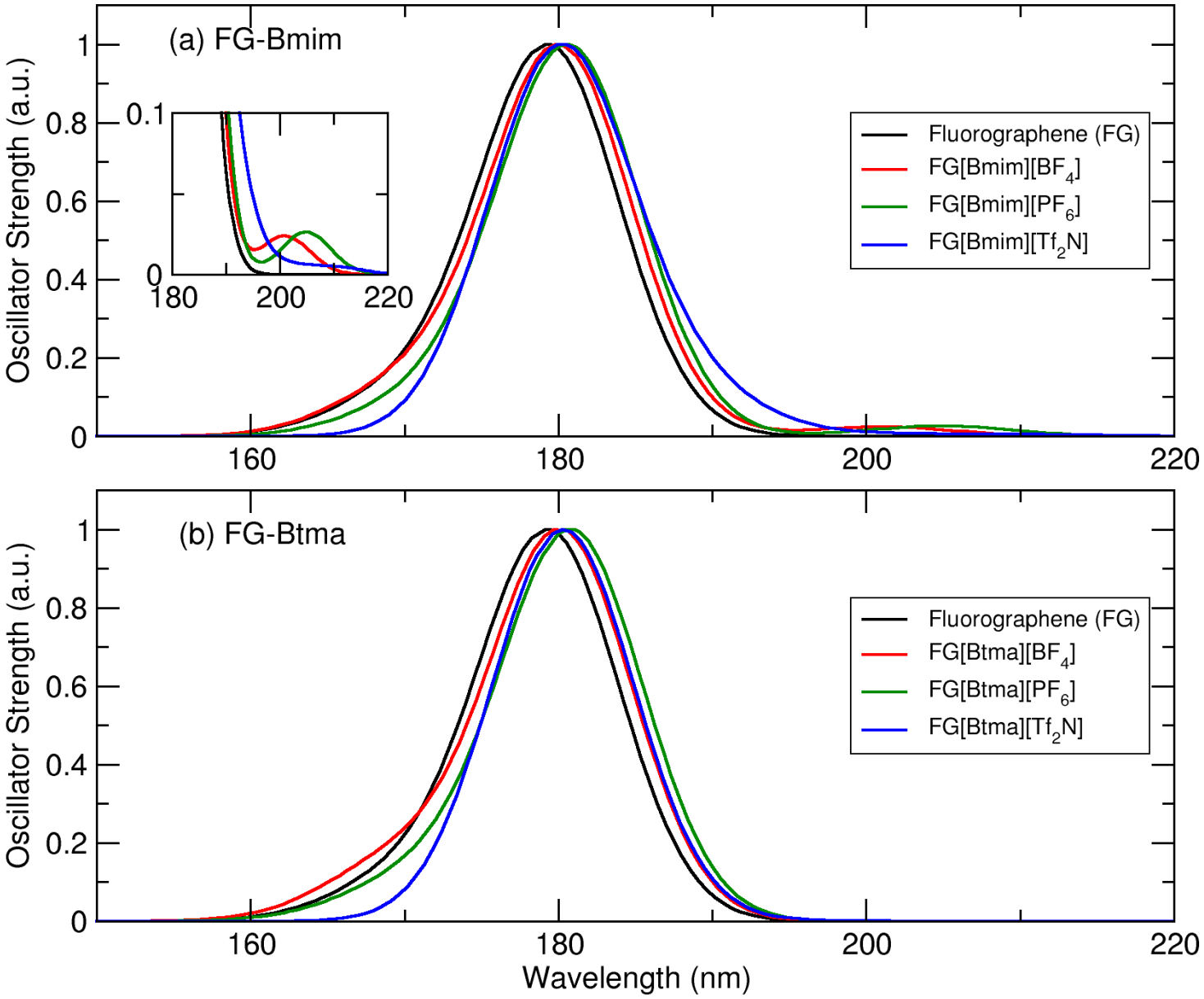
(a) FG-Bmim
Oscillator Strength (a.u.)
Fluorographene (FG)
FG[Bmim][BF4]
FG[Bmim][PF6]
FG[Bmim][Tf2N]
(b) FG-Btma
Fluorographene (FG)
FG[Btma][BF4]
FG[Btma][PF6]
FG[Btma][Tf2N]
Wavelength (nm)

Table 1. Thermodynamic parameters of the studied systems: ΔE_b is the BSSE corrected binding energy; $\sum\rho(r)_{(cation\ldots FG)}$ is the sum of the electron density at the BCPs between the cations of the ionic liquids and the FG surface; $\sum\rho(r)_{(anion..FG)}$ is the same but for the anionic counterions; Δq(Surface) is the calculated charge transfer on the FG surface in the FG…IL complexes compared to the unassociated FG surface; $\varepsilon_{(HOMO)}$ and $\varepsilon_{(LUMO)}$ are the energy of the orbitals, and the E_g is the calculated HOMO-LUMO energy gap of the FG and FG…IL complexes; ΔE_g represents the decrease in the E_g for the FG-IL complexes relative to FG alone; E_{FL} represents the Fermi energy level; WF is the work function of the FG surface and FG…IL complexes; and ΔWF is the change of work function of FG surface upon the IL adsorption.

Structure	ΔE_b (kcal/mol)	$\sum\rho(r)_{(cation\ldots FG)}$	$\sum\rho(r)_{(anion..FG)}$	[a]$\Delta q_{(Surface)}$ (e)	$\varepsilon_{(HOMO)}$ (eV)	$\varepsilon_{(LUMO)}$ (eV)	[b]E_g (eV)	[c]ΔE_g (eV)	E_{FL} (eV)	WF (ev)	[d]ΔWF (eV)
Fluorographene					-10.86	-1.65	9.21		-6.25	6.25	
FG[Bmim][BF_4]	-2.02	0.0782	0.0558	-0.0898	-9.12	-1.57	7.55	-1.66	-5.34	5.34	-0.91
FG[Bmim][PF_6]	-2.28	0.0825	0.0760	-0.0401	-9.29	-1.81	7.48	-1.73	-5.55	5.55	-0.7
FG[Bmim][Tf_2N]	-2.31	0.0798	0.0544	-0.1824	-8.79	-1.79	7.0	-2.21	-5.29	5.29	-0.96
FG[Btma][BF_4]	-1.68	0.0629	0.0786	-0.0843	-10.57	-1.5	9.07	-0.14	-6.03	6.03	-0.22
FG[Btma][PF_6]	-1.98	0.0556	0.079	0.0294	-10.59	-1.8	8.79	-0.42	-6.19	6.19	-0.06
FG[Btma][Tf_2N]	-2.18	0.0931	0.0746	-0.0022	-8.94	-1.82	7.12	-2.09	-5.38	5.38	-0.87

[a] The charge on the fluorographene (FG) surface is zero before adsorption of ILs.

[b] $E_g = \varepsilon_{(LUMO)} - \varepsilon_{(HOMO)}$.

[c] $\Delta E_g = E_{g(FG\text{-}IL)} - E_{g(FG)}$.

[d] $\Delta WF = WF_{(FG\text{-}IL)} - WF_{(FG)}$